Redox Biology 77 (2024) 103362

Contents lists available at ScienceDirect

Redox Biology

journal homepage: www.elsevier.com/locate/redox

LncRNA-HMG incites colorectal cancer cells to chemoresistance via repressing p53-mediated ferroptosis

Zechang Xin [a], Chenyu Hu [a], Chunfeng Zhang [b], Ming Liu [a], Juan Li [a], Xiaoyan Sun [a], Yang Hu [a], Xiaofeng Liu [a,*], Kun Wang [c,**]

[a] Key Laboratory of Carcinogenesis and Translational Research (Ministry of Education/Beijing), Hepatopancreatobiliary Surgery Department I, Peking University Cancer Hospital & Institute, Beijing, 100142, China
[b] Department of Medical Genetics, School of Basic Medical Sciences, Peking University Health Science Center, Beijing, 100191, China
[c] State Key Laboratory of Holistic Integrative Management of Gastrointestinal Cancers, Beijing Key Laboratory of Carcinogenesis and Translational Research, Hepatopancreatobiliary Surgery Department I, Peking University Cancer Hospital & Institute, Beijing, 100142, China

ARTICLE INFO

Keywords:
LncRNA-HMG
Colorectal cancer
Chemoresistance
Ferroptosis
p53

ABSTRACT

Upon chemotherapy, excessive reactive oxygen species (ROS) often lead to the production of massive lipid peroxides in cancer cells and induce cell death, namely ferroptosis. The elimination of ROS is pivotal for tumor cells to escape from ferroptosis and acquire drug resistance. Nevertheless, the precise functions of long non-coding RNAs (lncRNAs) in ROS metabolism and tumor drug-resistance remain elusive. In this study, we identify LncRNA-HMG as a chemoresistance-related lncRNA in colorectal cancer (CRC) by high-throughput screening. Abnormally high expression of LncRNA-HMG predicts poorer prognosis in CRC patients. Concurrently, we found that LncRNA-HMG protects CRC cells from ferroptosis upon chemotherapy, thus enhancing drug resistance of CRC cells. LncRNA-HMG binds to p53 and facilitates MDM2-mediated degradation of p53. Decreased p53 induces upregulation of SLC7A11 and VKORC1L1, which contribute to increase the supply of reducing agents and eliminate excessive ROS. Consequently, CRC cells escape from ferroptosis and acquire chemoresistance. Importantly, inhibition of LncRNA-HMG by anti-sense oligo (ASO) dramatically sensitizes CRC cells to chemotherapy in patient-derived xenograft (PDX) model. LncRNA-HMG is also a transcriptional target of β-catenin/TCF and activated Wnt signals trigger the marked upregulation of LncRNA-HMG. Collectively, these findings demonstrate that LncRNA-HMG promotes CRC chemoresistance and might be a prognostic or therapeutic target for CRC.

1. Introduction

Colorectal cancer (CRC) is one of the most popular malignancies all over the world. In the past decades, the application of anticancer drugs (5-fluorouracil or oxaliplatin as the first-line drugs) monotherapy or combined regimens has markedly prolonged the survival time of advanced CRC patients [1,2]. However, frequent occurrence of chemoresistance causes important limitations to pharmacological therapy [3]. This urges us to uncover the key molecules and elucidate potential mechanisms responsible for chemoresistance in order to develop new therapeutic strategies.

Usually, tumor cells are shown to carry more reactive oxygen species (ROS) than their normal counterparts [4]. However, excessive ROS lead to the production of massive lipid peroxides, which give rise to lipid membrane dysregulation as well as cause cell death, defined as ferroptosis [5]. Upon chemotherapy or radiotherapy, a large number of ROS are produced to help kill cancer cells [6,7]. In chemoresistant cancer cells, it's important to eliminate ROS or lipid peroxides for protecting cells from ferroptosis and acquiring drug resistance [8]. The study of the cooperative mechanisms underlying ROS balance and cancer chemoresistance will bring us a better cognition about tumor treatment.

Metabolic alteration is critical for tumor cells to balance the production and elimination of ROS [9]. The reducing agents are regularly employed to detoxify ROS or lipid peroxides in order to keep cell survival, such as glutathione (GSH), and reduced nicotinamide adenine dinucleotide phosphate oxidase (NADPH) [10,11]. GSH assists GPX4 to

* Corresponding author.
** Corresponding author.
E-mail addresses: liuxiaofeng100@bjmu.edu.cn (X. Liu), wang-kun@bjmu.edu.cn (K. Wang).

https://doi.org/10.1016/j.redox.2024.103362
Received 13 August 2024; Received in revised form 11 September 2024; Accepted 17 September 2024
Available online 18 September 2024

transform lipid peroxides into non-toxic lipid alcohol, thereby suppressing ferroptosis [12]. The synthesis of cellular GSH depends on cystine transporter system xc- (mainly consisting of SLC7A11), which is essential for GPX4-mediated ferroptosis prevention [13]. Tumor suppressor, p53, transcriptionally inhibits expression of SLC7A11 to initiate ferroptosis [14]. Recently, it's reported that p53 also regulates vitamin K metabolism and induces ferroptosis [15]. VKORC1L1 is the critical enzyme for producing the reduced form of vitamin K to decrease lipid peroxides and protect cells from ferroptosis [16]. Activation of p53 reduces the expression of VKORC1L1, thus inducing cancer cell ferroptosis for tumor suppression. These studies indicated that p53-mediated metabolic alteration is connected with tumor suppression. For chemoresistant cells, evasion from p53-related ferroptosis is essential for gaining resistance to chemotherapy, which generates redundant ROS and lipid peroxides. However, the underlying mechanism remains elusive.

Long non-coding RNAs (lncRNAs) are defined as the non-coding RNA transcripts with a length of more than 200 nucleotides. Recently, a large number of studies have reported that lncRNAs are tightly associated with tumorigenesis and cancer progression such as cancer cell growth,

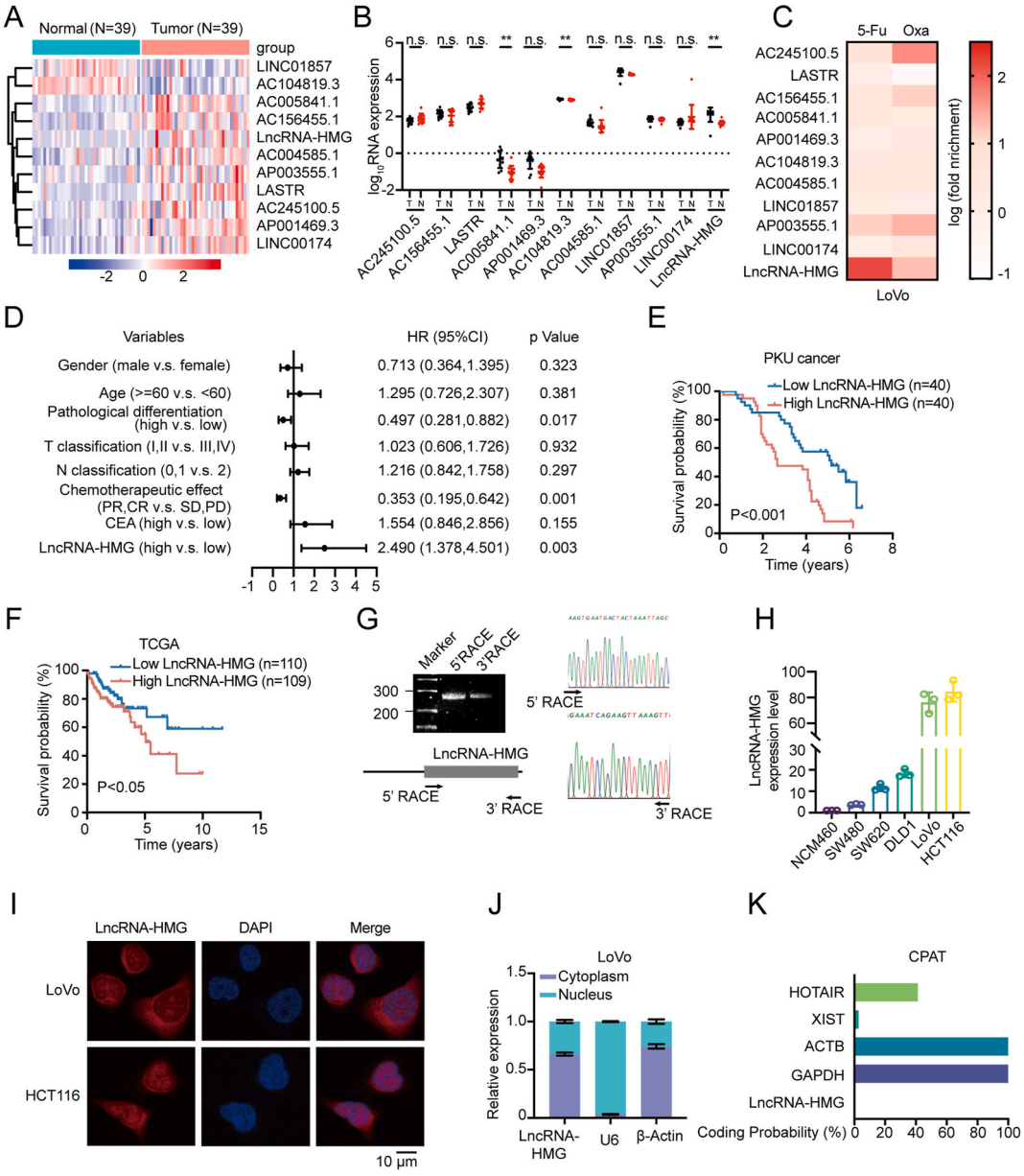

Fig. 1. LncRNA-HMG is associated with the prognosis of CRC patients. **A** The expression level of 11 lncRNAs in TCGA colon cancer patients (normal = 39, tumor = 39) was shown. **B** The expression levels of 11 lncRNAs in CRC tissues and adjacent tissues from Peking University Cancer hospital (PKU Cancer, normal = 12, tumor = 12) were detected. **C** The expression levels of 11 lncRNAs were detected by RT-qPCR in 5-Fu resistant and oxaliplatin-resistant cells. **D** The Cox regression analysis was employed for multivariate analyses of various prognostic parameters in CRC patients (PKU Cancer cohort). **E** Overall survival analysis based on LncRNA-HMG level was analyzed using data from PKU Cancer cohort. **F** Overall survival analysis based on LncRNA-HMG level was analyzed using data from TCGA colon cancer cohort. **G** The 5′ and 3′ rapid amplification of cDNA ends (RACE) assays in LoVo cells were performed for the comprehensive detection of the entire sequence of LncRNA-HMG. On the left, a gel electrophoresis image illustrated the PCR products obtained from the 5′-RACE and 3′-RACE assays. On the right, sequencing of these PCR products revealed the precise boundary between the universal anchor primer and the sequences specific to LncRNA-HMG. **H** The expression levels of LncRNA-HMG were detected by RT-qPCR in CRC cell lines (n = 3). **I** Subcellular localization of LncRNA-HMG was analyzed by FISH. **J** RT-qPCR detection of LncRNA-HMG expression in the cytoplasmic and nuclear fractions (n = 3). **K** The coding probability of GSCAR was predicted by CPAT (http://lilab.research.bcm.edu/). All the data are presented as mean ± S.D. *P < 0.05, **P < 0.01, ***P < 0.001.

metastasis, and drug resistance [17–19]. Targeting lncRNAs displays the potential to develop novel strategies for cancer treatment such as inhibiting lncRNAs by small interfering RNAs (siRNAs), antisense oligonucleotides (ASOs), or the CRISPR/Cas9 system [20,21]. It's reported that some lncRNAs are involved in regulating tumor metabolism. However, the roles of lncRNAs in modulating p53-mediated metabolic adaption to balance ROS level upon CRC chemotherapy are still unclear.

In our study, we found that LncRNA-HMG aggravates CRC chemoresistance. Mechanistically, LncRNA-HMG, induced by Wnt/β-catenin signaling, disrupts p53-mediated transcriptional repression to eliminate ROS and lipid peroxides, thereby suppressing ferroptosis. These findings uncover the pivotal roles of LncRNA-HMG in CRC chemoresistance and imply its potential value as a treatment target in CRC treatment.

2. Results

2.1. LncRNA-HMG is identified as a novel ferroptosis-related lncRNA

To dissect the ferroptosis-related lncRNA in CRC, we download TCGA data and performed the analysis as shown in Supplementary Fig. S1A. Finally, eleven lncRNAs were screened as the ferroptosis-related lncRNAs (Fig. 1A). Next, the expression of these 11 lncRNAs was evaluated in patients with CRC in another cohort (Peking University Cancer Hospital, PKU Cancer). As shown in Fig. 1B, three lncRNAs were increased in CRC tissues compared with the adjacent non-cancerous tissues, including AC005841.1, AC104819.3 and AC107308.1 (we referred it as LncRNA-HMG since it located near to *HMG* gene on chromosome). We also established the drug resistant CRC cells (Supplementary Fig. S1B) and analyzed the expression of these lncRNAs. Two lncRNAs were upregulated in 5-Fu (fluorouracil) resistant cells (AP003555.1 and LncRNA-HMG) and four lncRNAs were overexpressed in oxaliplatin resistant cells (AC245100.5, AC156455.1, AP003555.1 and LncRNA-HMG) (Fig. 1C). Since LncRNA-HMG was upregulated in all these analyses, we explored the functions of LncRNA-HMG in CRC chemoresistance and ferroptosis.

2.2. LncRNA-HMG expression level predicts the poor prognosis of CRC

Next, we evaluated the relationship between LncRNA-HMG level and prognosis of CRC patients. As shown in Fig. 1D, univariate analysis and multivariate Cox regression analyses revealed that besides chemotherapeutic effect, the level of LncRNA-HMG was also screened as an independent prognostic indicator for CRC patients (Fig. 1D and Tables S1–3). High LncRNA-HMG level was associated with a shorter overall survival in CRC patients in PKU cancer cohort (Fig. 1E). Moreover, the survival analysis using the TCGA dataset confirmed that high LncRNA-HMG expression indicated a worse overall survival in patients with CRC (Fig. 1F). Together, our data suggested that LncRNA-HMG is increased in CRC tissues and predicts a poor prognosis for CRC patients.

Through rapid amplification of the 5′ and 3' cDNA ends (RACE) assays, we successfully obtained the full length of LncRNA-HMG (Fig. 1G and Supplementary Fig. S1C). LncRNA-HMG was markedly upregulated in CRC cell lines compared to colon epithelial cell, NCM460 (Fig. 1H). RNA fluorescence in situ hybridization (FISH) assays were employed to determine the subcellular localization of LncRNA-HMG in CRC cells. The data revealed that LncRNA-HMG was localized in the cytoplasm, with some localization in the nucleus (Fig. 1I). The results were further confirmed by cytoplasmic and nuclear fraction analysis (Fig. 1J). In addition, we confirmed that LncRNA-HMG could not be translated into coding-proteins (Fig. 1K).

2.3. LncRNA-HMG protects CRC cells from ferroptosis

To investigate the biological role of LncRNA-HMG in ferroptosis, we inhibited the expression of LncRNA-HMG by specific shRNAs in HCT116 and LoVo cells, and cells expressing scrambled shRNA were used as controls (Fig. 2A). Erastin was frequently employed to induce ferroptosis [22]. Inhibition of LncRNA-HMG sensitized cells to erastin-induced death (Fig. 2B). Colony formation analysis further confirmed that downregulation of LncRNA-HMG sensitized cells to erastin (Fig. 2C). To verify the results, we generated LncRNA-HMG-overexpressing cells (Fig. 2D). Consistently, LncRNA-HMG overexpression attenuates erastin-induced cell death (Fig. 2E and F).

Ferroptosis is a lipid peroxidation-driven cell death cascade in an iron-dependent way [23]. Thus, we evaluated the lipid peroxidation and ROS level after LncRNA-HMG depletion. Knockdown of LncRNA-HMG upregulated ROS and lipid peroxidation of CRC cells (Fig. 2G and H). Notably, the intracellular GSH/GSSG ratio was decreased in LncRNA-HMG-depleted cells (Fig. 2I). To verify the results, the lipid ROS level was also analyzed by C11-BODIPY and flow cytometry analysis. As shown in Fig. 2J, LncRNA-HMG depletion upregulated ROS level of CRC cells. Furthermore, in LncRNA-HMG-overexpressing cells, ROS and lipid peroxidation was significantly downregulated while GSH was upregulated (Fig. 2K–M). Transmission electron microscopy (TEM) analysis suggested that mitochondria in LncRNA-HMG-depleted cells showed obvious characteristic of ferroptosis, displaying mitochondrial atrophy, reduction of mitochondrial size, and smaller cristae (Fig. 2N). Together, these data suggested that LncRNA-HMG suppresses ferroptosis of CRC cells.

2.4. LncRNA-HMG promotes chemoresistance of CRC cells

Next, we explored the roles of LncRNA-HMG in CRC progression. As shown in Fig. 3A and B, LncRNA-HMG depletion decreased cell proliferation and colony formation. Consistently, LncRNA-HMG overexpression enhanced cell proliferation and colony formation (Supplementary Figs. S2A and S2B). The response of LncRNA-HMG-depleted cells to 5-Fu or oxaliplatin was further evaluated. Inhibition of LncRNA-HMG sensitized the CRC cells to 5-Fu or oxaliplatin treatment (Fig. 3C and Supplementary Fig. S2C). In drug-resistant cells, knockdown of LncRNA-HMG also improved chemosensitivity of these cells (Supplementary Fig. S2D). Overexpression of LncRNA-HMG enhanced chemoresistance of CRC cells (Fig. 3D and Supplementary Fig. S2E). Colony formation analysis confirmed these results (Fig. 3E and F). Together, these data indicated that LncRNA-HMG enhances chemoresistance of CRC cells.

Upon chemotherapy, cancer cells are often exposed to high level of ROS, which causes lipid peroxidation and ferroptosis. Since LncRNA-HMG plays important role in eliminating ROS in cancer cells, we hypothesize that LncRNA-HMG enhances chemoresistance by decreasing ROS level after drug treatment. However, the lipid ROS level was grammatically elevated in LncRNA-HMG-depleted cells upon drug treatment (Fig. 3G and Supplementary Fig. S2F). Accordingly, LncRNA-HMG changed the intracellular GSH/GSSG ratio upon chemotherapy (Fig. 3H and I). Meanwhile, TEM results confirmed that LncRNA-HMG alleviated drug-induced dysfunction of mitochondria in CRC cells (Fig. 3J). Ferrostatin-1, a ferroptosis inhibitor, reversed cell death caused by LncRNA-HMG shRNA upon chemotherapy (Supplementary Fig. S2G). Thus, these data revealed that LncRNA-HMG increases the production of reducing substance and impairs drug-induced ferroptosis, thereby decreasing chemosensitivity of CRC cells.

2.5. LncRNA-HMG weakens p53-mediated ferroptosis

To explore the related molecular mechanisms underlying LncRNA-HMG-mediated chemoresistance of CRC cells, we analyzed the potential LncRNA-HMG-involved pathways. According to the LncRNA-HMG level, CRC samples were divided into two groups, including the LncRNA-HMG-low group and the LncRNA-HMG-high group. Next, we identified the differentially expressed genes (DEGs) between the two groups (Fig. 4A). The gene enrichment analysis demonstrated that these genes were significantly enriched in gene sets related to p53 signaling

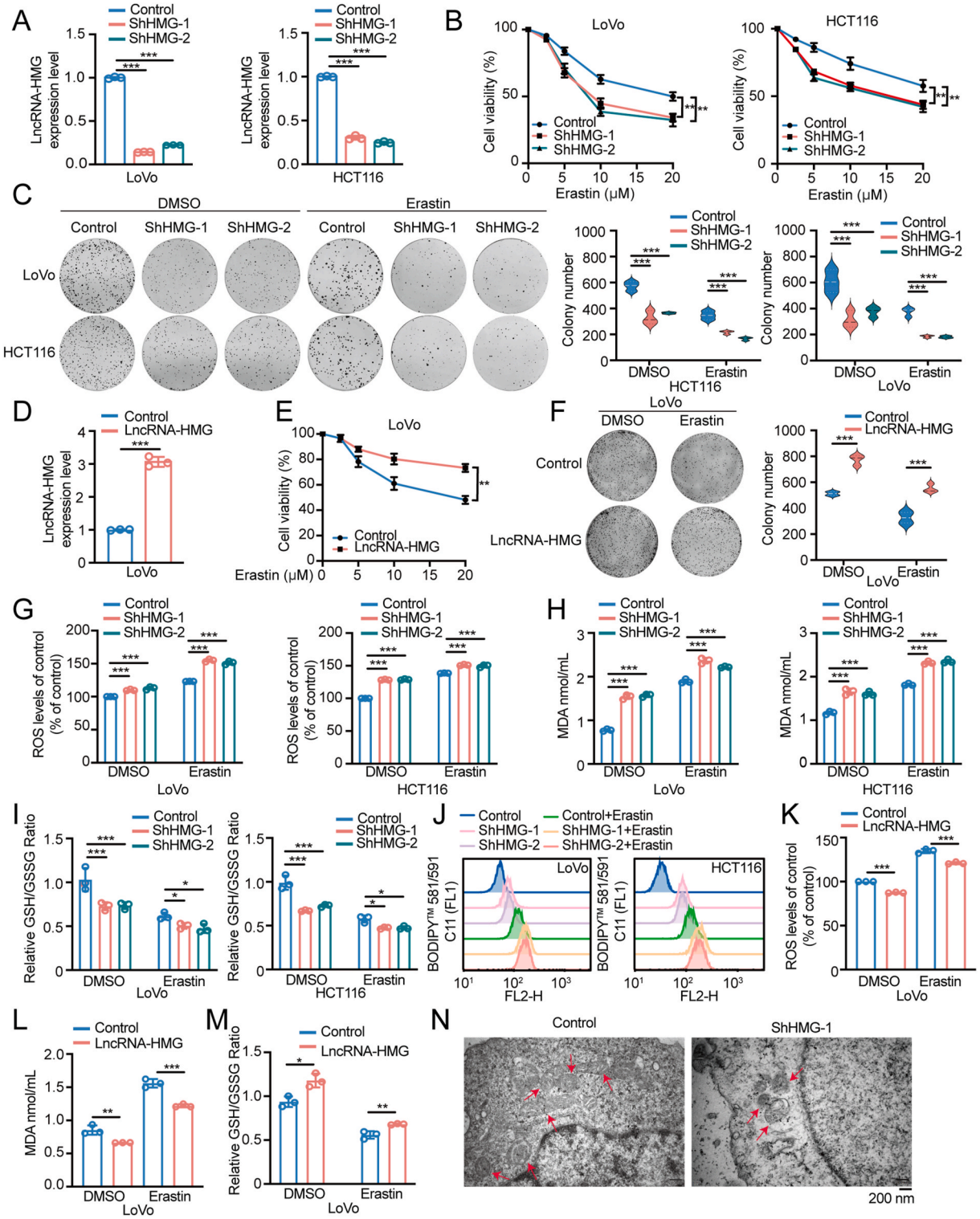

Fig. 2. The LncRNA-HMG protects CRC cells from ferroptosis. **A** The stable LncRNA-HMG knockdown cell line was established and LncRNA-HMG level was assessed by RT-qPCR (n = 3). **B** The proliferation capacity of cells stably expressing shHMG treated with different concentrations of Erastin (5 μM) for 8 h was examined using the cell counting kit (CCK-8) kit (n = 4). **C** The indicated cells were treated or untreated with Erastin (5 μM) and cell colony formation experiments were performed. The results were summarized using data derived from three independent experiments (n = 3). **D** The cells stably expressing LncRNA-HMG were constructed and LncRNA-HMG level was evaluated by RT-qPCR (n = 3). **E** The proliferation capacity of the indicated cells treated with different concentrations of Erastin was assessed (n = 4). **F** The colony formation experiment was performed using the indicated cells and results derived from three independent experiments were presented in a violin plot (n = 3). **G** The relative level of ROS was detected in the indicated cells (n = 3). **H** The lipid peroxidation level was analyzed in the indicated cells. **I** GSH/GSSG ratio was detected in the indicated cells after Erastin (5 μM) treatment (n = 3). **J** C11-BODIPY level was analyzed in the indicated cells (n = 3). **K-M** The ROS level (K), lipid peroxidation level (L), and GSH/GSSG ratio (M) were analyzed in LncRNA-HMG-overexpressed CRC cells as indicated (n = 3). **N** The indicated cells were subjected to TEM. Representative TEM images of mitochondrial morphology were presented. Red arrows indicate the mitochondria. All the data are presented as mean ± SD. *P < 0.05, **P < 0.01, ***P < 0.001.

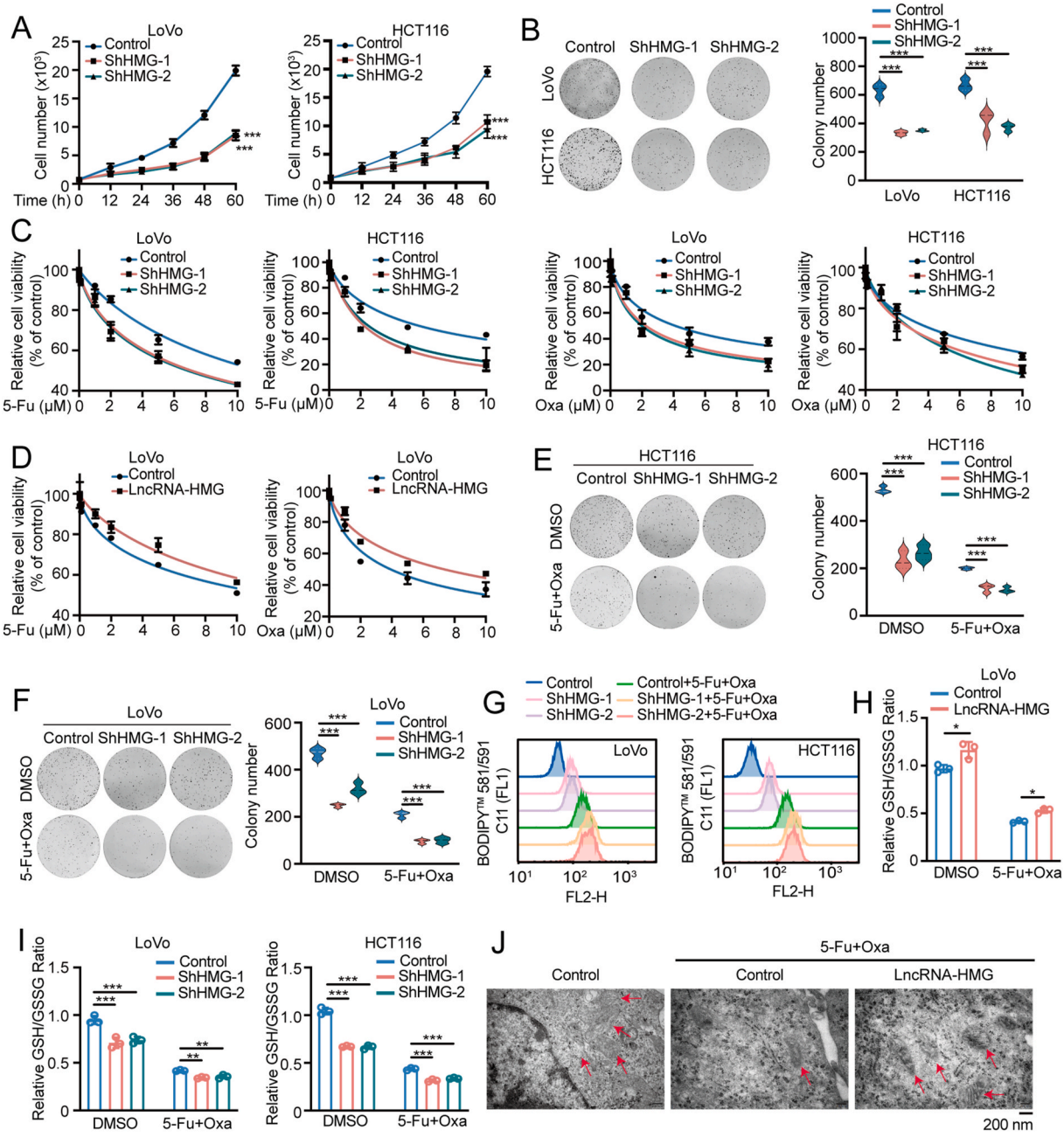

Fig. 3. LncRNA-HMG promotes the drug resistance of CRC Cells. **A** The proliferation capacity of cells stably expressing LncRNA-HMG was assessed by CCK-8 experiment (n = 4). **B** The cell colony formation experiment was conducted with the indicated cells (n = 3). **C** The IC_{50} values of the indicated cells were detected after treatment of the indicated drugs (n = 3). **D** The IC_{50} values of the cells overexpressing LncRNA-HMG were detected after treatment of the indicated drugs (n = 3). **E-F** The colony formation experiment was conducted with the indicated cells treated or untreated with 5-Fu (5 μM) and oxaliplatin (40 μM) for 24 h. The results were summarized with the data derived from three independent experiments (n = 3). **G** ROS level was analyzed by C11-BODIPY assay in LncRNA-HMG-depleted cells treated or untreated with 5-Fu (5 μM) and oxaliplatin (40 μM) for 24 h (n = 3). **H** GSH/GSSG ratio was detected in LncRNA-HMG overexpressed CRC cells (n = 3). **I** The indicated cells were harvested and GSH/GSSG ratio was analyzed (n = 3). **J** The indicated cells were treated with or without 5-Fu (5 μM) and oxaliplatin (40 μM) for 24 h. Then, TEM was employed to analyze the mitochondrial morphology. Red arrows indicate the mitochondria. All the data are presented as mean ± SD. *P < 0.05, **P < 0.01, ***P < 0.001.

(Fig. 4B and Supplementary Fig. S3A). Recently, p53 signaling is reported to be involved in regulating ferroptosis [24]. Next, we purified LncRNA-HMG-binding proteins and mass spectrometry analysis was conducted to identify these proteins. Totally, 104 proteins were identified as LncRNA-HMG-binding proteins (Table S4). Protein-protein interaction analysis by STRING screened the top 25 hub genes among the 104 proteins (Fig. 4C), indicating that p53 is one of the hub factors. Together, it's possible that LncRNA-HMG binds to p53 and regulates p53 signaling pathway.

As a critical transcriptional factor, p53 affects the intracellular ROS level by inhibiting the expression of ferroptosis suppressors, such as SLC7A11 and VKORC1L1 [16]. Thus, we determined the p53 protein levels and its downstream targets after LncRNA-HMG ablation. As shown in Fig. 4D and Supplementary Fig. S3B, LncRNA-HMG depletion increased p53 level while decreased SLC7A11 and VKORC1L1 levels. Overexpression of LncRNA-HMG had an opposite effect on the level of these proteins (Fig. 4E). Furthermore, the mRNA levels of SLC7A11 and VKORC1L1 were decreased in LncRNA-HMG-depleted cells (Fig. 4F)

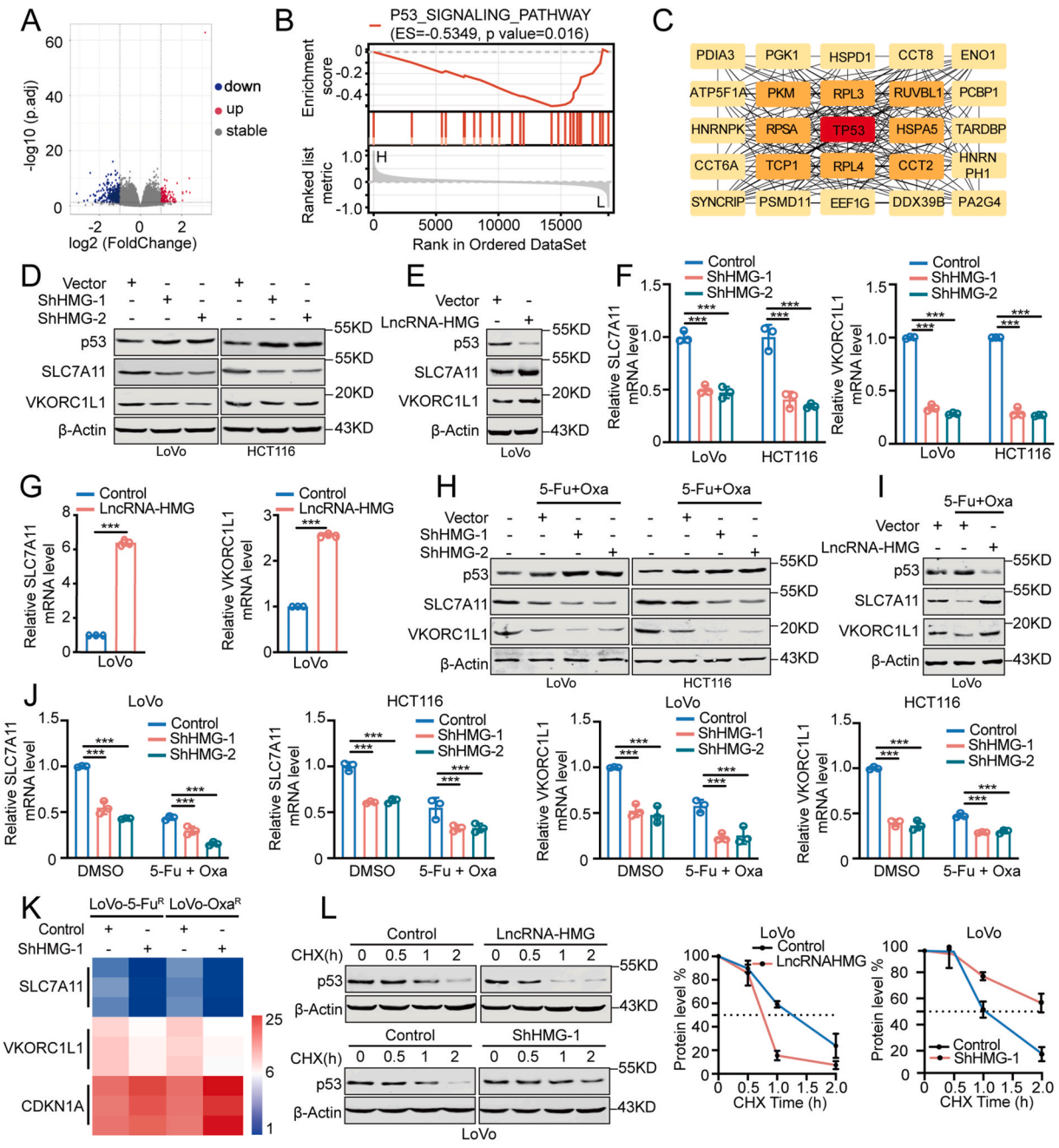

Fig. 4. LncRNA-HMG regulates the expression levels of SLC7A11 and VKORC1L1. **A** The differentially expressed genes were identified between LncRNA-HMG-high samples and LncRNA-HMG-low samples based on TCGA data. **B** Pathway enrichment analysis was performed with GSEA method and the result suggested that LncRNA-HMG was negatively correlated with p53 signaling. **C** LncRNA-HMG binding proteins were identified through mass spectrometry analysis and protein-protein interaction (PPI) analysis was employed to uncover the top 25 hub genes. **D** The control or shHMG cells were lysed and the indicated proteins were detected by Western blot. **E** LoVo cells were transfected with the indicated vectors and western bot was performed using the indicated antibodies. **F-G** The total RNA was extracted from the indicated cells and RT-qPCR was performed to detect the indicated genes (n = 3). **H–I** CRC cells were treated with 5-Fu (5 μM) and oxaliplatin (40 μM) for 24 h. Then, Western blot was performed using the indicated antibodies. **J** Relative mRNA expression levels of SLC7A11 and VKORC1L1 were detected by RT-qPCR in the indicated CRC cells treated with or without 5-Fu (5 μM) and oxaliplatin (40 μM) for 24 h (n = 3). **K** LncRNA-HMG was depleted in 5-Fu and oxaliplatin-resistant cells and RNA sequencing analysis was performed to analyze the indicated mRNA levels. **L** The indicated cells were treated with CHX (50 μg/mL) and the p53 level was analyzed by Western blot (n = 3). All the data are presented as mean ± SD. *P < 0.05, **P < 0.01, ***P < 0.001.

while were upregulated in LncRNA-HMG-overexpressed cells (Fig. 4G). These data indicated that LncRNA-HMG regulates p53 and its downstream targets.

Consistent with previous reports [25], p53 was upregulated in response to anti-tumor drug treatment (Supplementary Fig. S3C). Therefore, it's important to elucidate whether LncRNA-HMG affects p53 activation after drug treatment. As shown in Fig. 4H, LncRNA-HMG depletion promoted the elevation of p53 in response to 5-Fu and oxaliplatin treatment. However, overexpression of LncRNA-HMG declined p53 activation (Fig. 4I). Consistently, knockdown of LncRNA-HMG downregulated the expression of SLC7A11 and VKORC1L1 while overexpression of LncRNA-HMG enhanced the expression of these two targets (Fig. 4H, I and 4J). Additionally, we also observed the effect of LncRNA-HMG on other p53 targets, such as p21. As shown in

Supplementary Fig. S3D, the mRNA level of p21 was upregulated in LncRNA-HMG depleted cells. Moreover, LncRNA-HMG was depleted in chemoresistant cells and the expression of these three genes was examined by RNA-seqencing (RNA-seq). As shown in Fig. 4K, similar phenomenon was observed in chemoresistant CRC cells. To explore whether SLC7A11 and VKORC1L1 are required for LncRNA-HMG-repressed ferroptosis, we depleted the expression of SLC7A11 and VKORC1L1 in cells (Supplementary Fig. S3E). In these cells, knockdown of LncRNA-HMG had little effect on lipid peroxidation, indicating the critical roles of SLC7A11 and VKORC1L1 in LncRNA-HMG-repressed ferroptosis (Supplementary Fig. S3F). Intriguingly, LncRNA-HMG still regulated cell proliferation in SLC7A11/VKORC1L1-depleted cells (Supplementary Fig. S3G). Since LncRNA-HMG regulated the expression of p21, one of the most regulators in cell proliferation [26], it's possible that LncRNA-HMG-related cell proliferation mainly depends on inhibiting p21 expression. Thus, these data suggested that LncRNA-HMG regulates p53 level, further changing the expression of p53 downstream targets. The protein stability of p53 plays important roles in control p53 level [27]. The cycloheximide (CHX, a ribosome-stalling drug) was employed to block protein translation and the stability of p53 was further analyzed. As shown in Fig. 4L, p53 stability was compromised in LncRNA-HMG-overexpressed cells while inhibition of LncRNA-HMG enhanced the stability of p53. Together, our data revealed that LncRNA-HMG declines the stability of p53 and weakens p53-medicated ROS ferroptosis.

2.6. LncRNA-HMG assists MDM2 to increase ubiquitination of p53

We next investigated how LncRNA-HMG regulates p53 stability. The interaction between p53 and LncRNA-HMG was confirmed by RIP assay (Fig. 5A). The ubiquitin-proteasome system (UPS) is critical for modulating p53 stability [28]. Thus, the proteasome inhibitor, MG132, was utilized to analyze if LncRNA-HMG-related p53 stabilization relies on UPS. p53 elevation by LncRNA-HMG depletion was reversed by the addition of MG132, suggesting that LncRNA-HMG modulates p53 protein level in a proteasome-dependent manner (Fig. 5B). The ubiquitination level of p53 was decreased in LncRNA-HMG-depleted cells (Fig. 5C). Overexpression of LncRNA-HMG promoted the ubiquitination of p53 (Fig. 5D). These results suggested that LncRNA-HMG promotes ubiquitination of p53, leading to degradation of p53. It's important to analyze how LncRNA-HMG promotes ubiquitination of p53. MDM2 acts as the most important ubiquitin ligase for p53 [29]. It's possible that LncRNA-HMG enhances the activity of MDM2 to p53. To test this hypothesis, we firstly evaluated the interaction of LncRNA-HMG and MDM2. As shown in Fig. 5E, LncRNA-HMG binds to p53 and MDM2 simultaneously. The interaction of LncRNA-HMG and MDM2 was further verified by RIP assay (Fig. 5F). RNA pull-down assay further verified that LncRNA-HMG binds to p53 or MDM2 (Fig. 5G). Importantly, LncRNA-HMG had on effect on MDM2 level (Fig. 5H). Furthermore, we found that depletion of LncRNA-HMG reduced the interaction between p53 and MDM2 (Fig. 5I). LncRNA-HMG overexpression increased MDM2-mediated p53 ubiquitination (Fig. 5J). Moreover, Nutlin-3, the antagonist of MDM2, abrogated the effect of LncRNA-HMG on p53 protein level (Supplementary Fig. S4A). It's known that the phosphorylation or acetylation of p53 affects p53-MDM2 interaction [25]. We found that LncRNA-HMG had little effect on the phosphorylation or acetylation of p53, indicating the direct role of LncRNA-HMG on p53-MDM2 interaction (Supplementary Fig. S4B). Thus, these data suggested that LncRNA-HMG promotes the interaction of MDM2 with p53 and enhances ubiquitination of p53.

It's unknown whether LncRNA-HMG regulates ROS state relying on p53. To address this issue, we employed HCT116 p53 null cells and generated LncRNA-HMG depleted cells (Supplementary Fig. S4C and Fig. 5K). LncRNA-HMG had little effect on the expression level of SLC7A11 (Fig. 5L and M) and the intracellular GSH/GSSG ratio (Fig. 5N). We also overexpressed LncRNA-HMG in p53 null cells (Fig. 5O). The expression level of SLC7A11 showed no changes even if LncRNA-HMG was overexpressed in p53 null cells (Fig. 5P and Q). The similar phenomena were observed when we detected GSH/GSSG ratio (Fig. 5R). These findings indicated that LncRNA-HMG modulates ROS state depending on p53.

2.7. Inhibition of LncRNA-HMG sensitizes CRC cells to chemotherapy in vivo

Next, we analyzed the role of LncRNA-HMG in CRC chemoresistance *in vivo*. LncRNA-HMG-depleted or control cells were implanted into nude mice. LncRNA-HMG attenuated tumor growth in mice xenografts (Fig. 6A and B and Supplementary S5A). The expression of Ki67 and SLC7A11 was also decreased in LncRNA-HMG-depleted cells (Fig. 6C). We next determined if LncRNA-HMG modulates the chemosensitivity of CRC cells *in vivo*. Tumor with LncRNA-HMG depletion was more sensitive to 5-Fu or oxaliplatin when compared with control group, revealing that LncRNA-HMG suppressed the chemosensitivity of CRC cells (Fig. 6A and B and Supplementary Fig. S5A). The expression of SLC7A11 and VKORC1L1 was detected in xenograft tissues. As shown in Fig. 6C and Supplementary Fig. S5B, p53 was elevated while SLC7A11 and VKORC1L1 were decreased when LncRNA-HMG was abrogated.

Next, we established the patient-derived xenograft (PDX) models using tumor tissues from CRC patients carrying wild-type p53 (Fig. 6D). The *in vivo*-optimized LncRNA-HMG inhibitor (LncRNA-HMG ASO) was used to treat cancer combined with chemotherapy (Supplementary Fig. S5C). LncRNA-HMG ASO downregulated the expression of LncRNA-HMG in PDX model (Supplementary Fig. S5D). As shown in Fig. 6E and F, LncRNA-HMG ASO significantly reduced tumor growth and increased the chemosensitivity in PDX model. Accordingly, as shown in the IHC and Western blot analyses, LncRNA-HMG knockdown affected cell proliferation (indicated by Ki67) and downregulated the expression of SLC7A11 and VKORC1L1 (Fig. 6G and Supplementary S5E). Together, these data suggested that LncRNA-HMG inhibitor promotes chemosensitity of CRC.

2.8. LncRNA-HMG is a transcriptional target of β-catenin

Because LncRNA-HMG is highly expressed in CRC, we tried to uncover the mechanism of LncRNA-HMG regulation. The potential transcriptional factors bound to the promoter region of LncRNA-HMG were predicted (Fig. 7A and Supplementary Fig. S6A). Among these factors, TCF4/β-catenin is of interest due to the importance of Wnt/β-catenin signaling in CRC progression [30]. β-catenin overexpression increased the expression level of LncRNA-HMG (Fig. 7B), suggested that Wnt/β-catenin regulated LncRNA-HMG. To confirm the results, we used β-catenin activator (LiCl) to treat cells. As shown in Fig. 7C, LiCl treatment upregulated LncRNA-HMG level. Moreover, iCRT14, a TCF4/β-catenin inhibitor [31], significantly downregulated the expression LncRNA-HMG (Fig. 7D). Thus, these data demonstrated that Wnt/β-catenin upregulates the expression of LncRNA-HMG. As expected, the LncRNA-HMG promoter contained TCF-binding elements (Fig. 7E), which was further verified by ChIP assay (Fig. 7F). Consistently, the transcriptional activity of luciferase reporters containing the region of LncRNA-HMG promoter was markedly upregulated by LiCl treatment or β-catenin overexpression while iCRT14 inhibited this effect (Fig. 7G). Together, these data suggested that LncRNA-HMG is a transcriptional target of β-catenin.

3. Discussion

Chemoresistance is one of the major issues hindering the improvement of the prognosis of CRC patients. In cancer cells, various metabolic pathways are often altered to support tumor survival [32,33]. In this study, we uncovered a novel lncRNA involved in drug resistance by

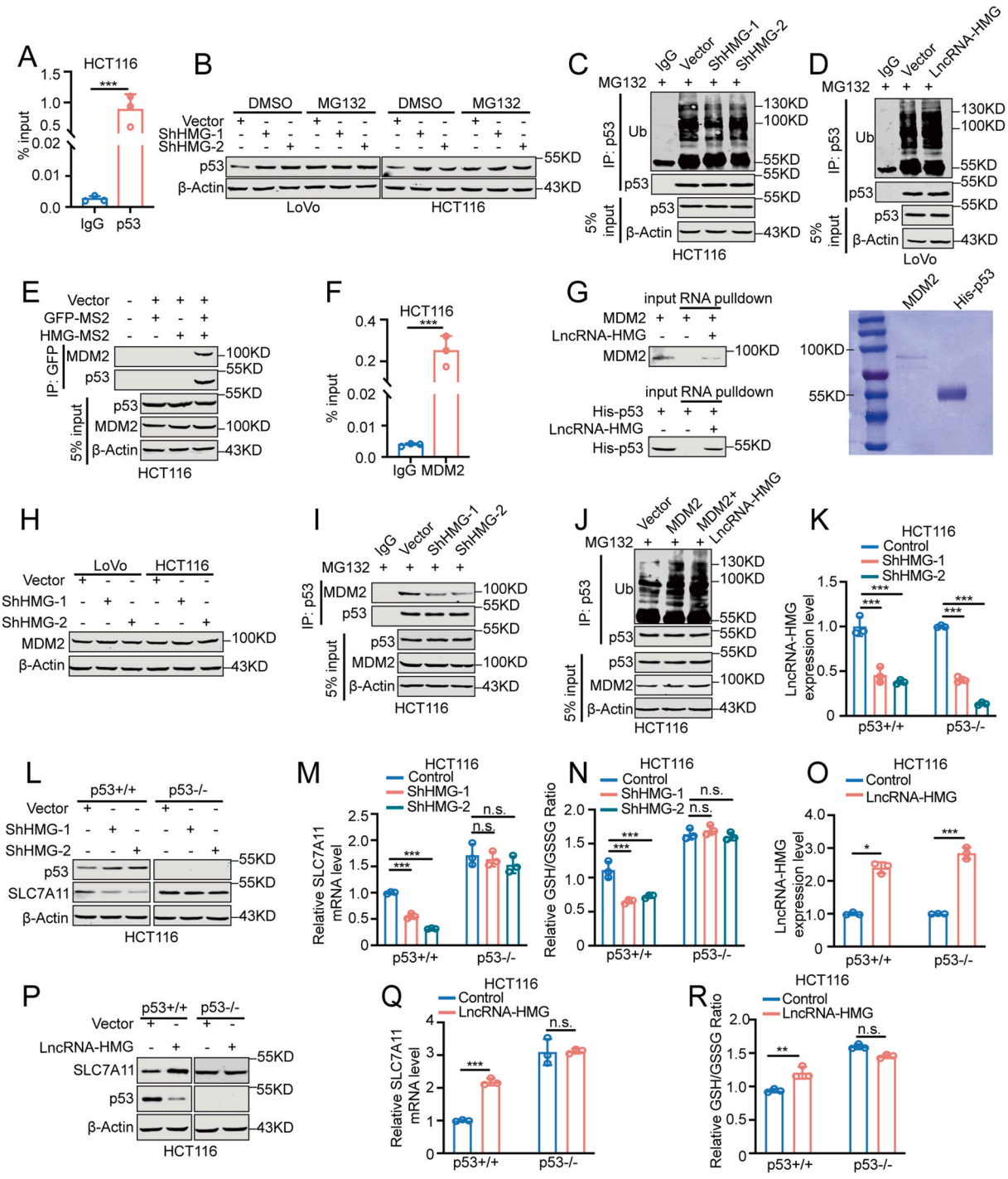

Fig. 5. LncRNA-HMG promotes p53 ubiquitination. **A** RIP analysis was performed using anti-p53 antibody and the immunoprecipitates were subjected to RT-qPCR for analyzing LncRNA-HMG level. **B** The indicated cells were treated with MG132 (10 μM) for 4 h, and the cell lysates were subjected to Western blot using the indicated antibodies. **C-D** Ubiquitination levels of p53 were analyzed in the indicated cells. **E** The GFP-MS2 and LncRNA-HMG-MS2 were transfected into HCT116 cells and LncRNA-HMG-binding proteins were subjected to Western blot using anti-p53 or anti-MDM2 antibodies. **F** RIP assay was performed using anti-MDM2 antibody and RT-qPCR was conducted to detect LncRNA-HMG level. **G** RNA-pull down assay was performed to analyze the direct binding of LncRNA-HMG to MDM2 or p53. **H** The control or LncRNA-HMG-depleted cells were harvested and Western blot was performed using the indicated antibodies. **I** The interaction between MDM2 and p53 was detected by immunoprecipitation in LncRNA-HMG depleted cells. **J** The cells were transfected with indicated vectors. Then, the ubiquitination level of p53 was evaluated using anti-p53 antibody. **K** LncRNA-HMG was depleted in HCT116 $p53^{+/+}$ or $p53^{-/-}$ cells and the knockdown efficiency was verified by RT-qPCR (n = 3). **L** The p53 and SLC7A11 levels were evaluated by Western blot in the indicated cells. **M** The mRNA level of SLC7A11 was detected by RT-qPCR in the indicated cells (n = 3). **N** GSH/GSSG ratio in the indicated cells was analyzed (n = 3). **O** The stable cells overexpressing LncRNA-HMG were established in HCT116 $p53^{+/+}$ or $p53^{-/-}$ cells. RT-qPCR was conducted to analyze the LncRNA-HMG level (n = 3). **P** The p53 and SLC7A11 levels were evaluated by Western blot in the indicated cells. **Q** The mRNA level of SLC7A11 was detected by RT-qPCR in the indicated cells (n = 3). **R** GSH/GSSG ratio in the indicated cells was analyzed (n = 3). All the data are presented as mean ± SD. *P < 0.05, **P < 0.01, ***P < 0.001.

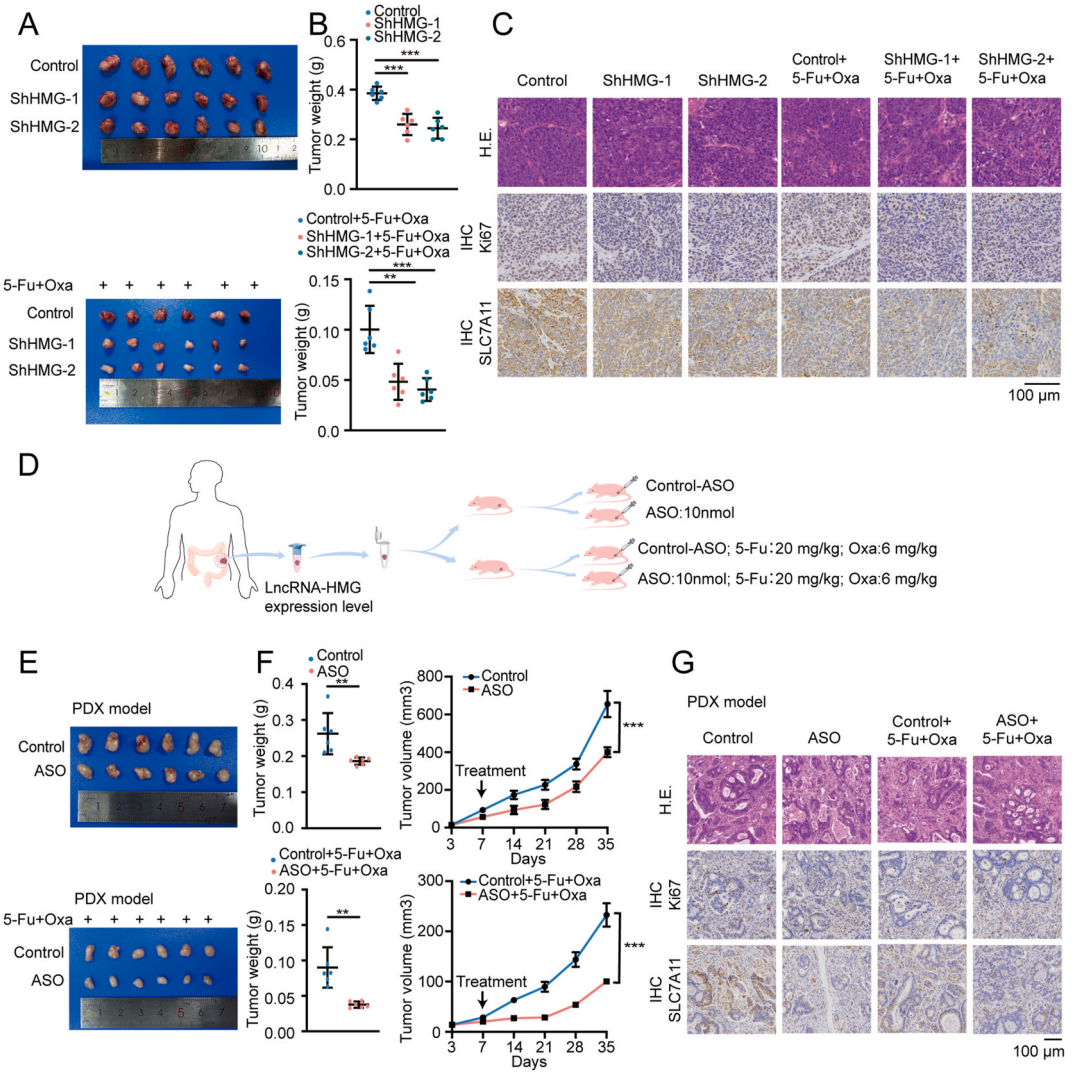

Fig. 6. Inhibition of LncRNA-HMG promotes chemosensitivity of CRC cells *in vivo*. **A** Tumor formation assay in nude mice injected with LncRNA-HMG-depleted cells or control LoVo cells was performed. The right group was treated with 5-Fu (20 mg/kg) and Oxaliplatin (6 mg/kg) as described in the methods part. **B** The xenograft tumor weight was summarized. **C** The Ki67 or SLC7A11 level xenograft tissues were evaluated by IHC. **D** The experiments were designed to test the effect of the combination of *in vivo*-optimized LncRNA-HMG ASO inhibitor and chemotherapy in CRC PDX models. Graphic illustration was shown. **E** The image of xenograft tumor in PDX model was presented after treated as indicated. **F** The statistical analysis of tumor growth and weight was performed in PDX model. **G** The Ki67 or SLC7A11 level in PDX xenograft tissues were evaluated by IHC. *P < 0.05, **P < 0.01, ***P < 0.001.

remodeling ROS elimination (Fig. 7H). LncRNA-HMG increases the supply of reducing agents by suppressing p53-mediated transcriptional regulation of SLC7A11 and VKORC1L1. This is helpful for cancer cells to escape from drug-induced ferroptosis and acquire chemoresistance. Moreover, LncRNA-HMG is transactivated by Wnt/β-catenin signaling. Notably, inhibition of LncRNA-HMG using specific ASO significantly sensitizes CRC cells to chemotherapy. Our data suggested the potential of LncRNA-HMG in treating CRC. However, it's unknown whether LncRNA-HMG is associated with cancer progression in other types of human cancers. It is important to further explore the expression of LncRNA-HMG in pan-cancer analysis and analyze the roles of LncRNA-HMG in other cancer treatment.

Tumor suppressor p53 is crucial to determinate cell fate upon cellular stress [34]. As a transcriptional factor, p53 modulates the transcription of diverse downstream genes in response to different stimuli, functioning in cell cycle arrest, DNA repair, apoptosis, and ferroptosis [26]. Recently, it's reported that p53 regulates ROS metabolism to promotes lipid peroxides and ferroptosis [35,36]. Dysfunction of p53 is tightly associated with cancer progression, and it's important to elucidate how p53 is dysregulated. MDM2 is a ubiquitin ligase which acts as a critical inhibitor of p53 [37]. Small molecules, such as RG7388, have been developed to restore p53 signaling and treat human cancers [38]. Here, we identified LncRNA-HMG as a linker of MDM2 and p53 in CRC cells. LncRNA-HMG largely promotes MDM2-mediated p53 degradation, leading to anti-ferroptosis of cancer cells upon chemotherapy. Our findings indicate the complexity of p53 regulatory mechanism. Besides small molecules, the inhibitors targeting lncRNAs might be alternative strategy to restore p53 signaling in cancer treatment.

Besides p53, LncRNA-HMG also binds to other proteins, such as ENO1, HSPA5, and RUVBL1. ENO1 regulates ferroptosis in cancer cell via modulating AKT/STAT3 signaling [39]. HSPA5 inhibits ferroptosis by maintaining GPX4 stability [40]. RUVBL1 is also involved in CRC progression [41]. Even if we uncovered the roles of LncRNA-HMG in CRC chemoresistance, the knowledge about the functions of LncRNA-HMG in cancer is still little. It's possible that LncRNA-HMG also binds to the proteins, like ENO1 and HSPA5, to regulate CRC progression. This needs to be investigated in the future.

Wnt/β-catenin signaling pathway plays important roles in CRC progression [42]. Upon Wnt signals, accumulated β-catenin translocates into the nucleus and helps TCF transcription factors activate the

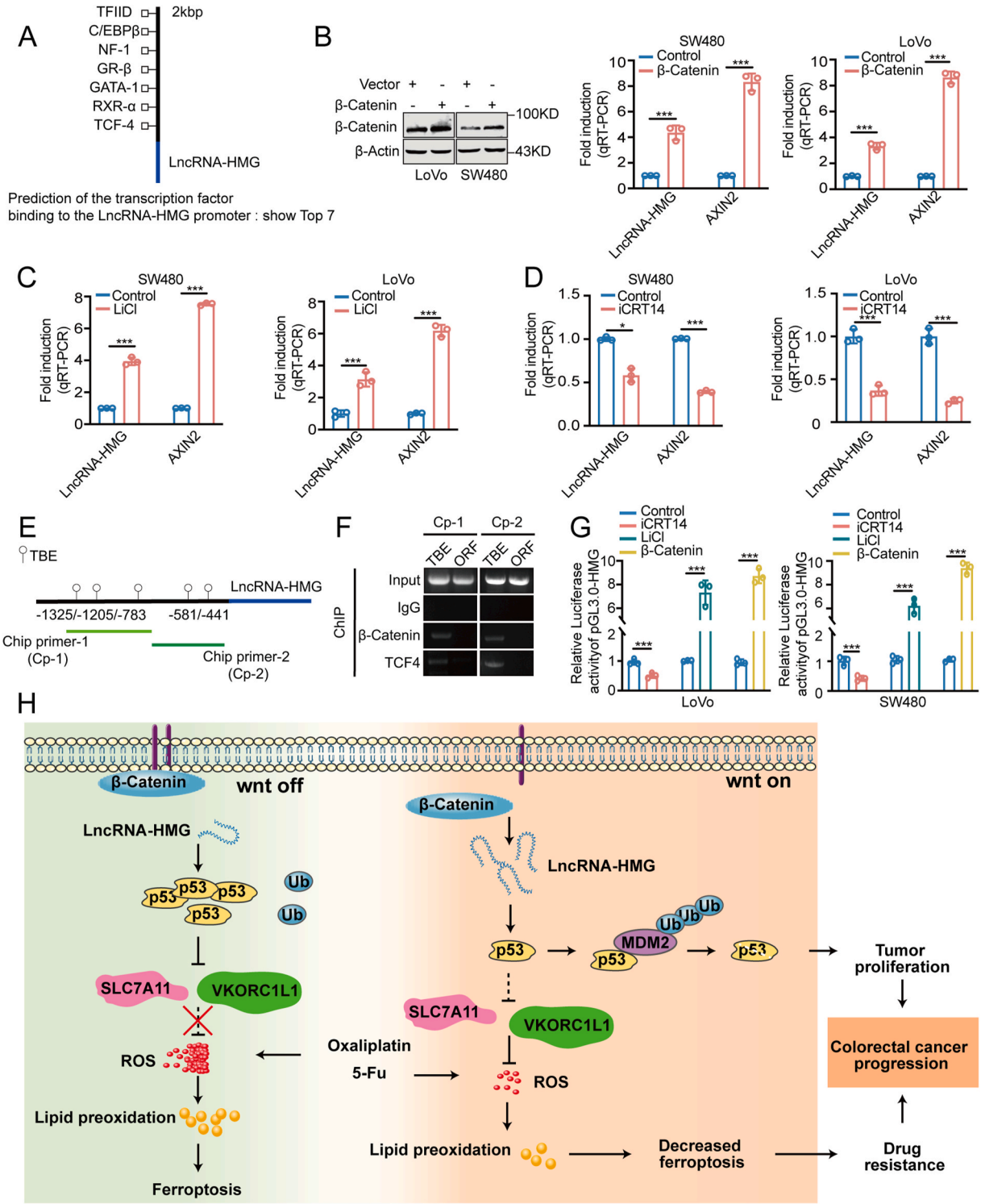

Fig. 7. LncRNA-HMG is a transcriptional target of Wnt/β-catenin signaling. **A** The prediction of the transcription factor binding to the LncRNA-HMG promoter using the PROMO database. **B** Cells were transfected as indicated and total RNA was extracted. RT-qPCR was performed using the indicated primers (n = 3). **C** Cells were treated with LiCl (10 mmol/L) for 24 h. Then, LncRNA-HMG was analyzed by RT-qPCR (n = 3). **D** Cells were treated with iCRT14 (50 μM) for 24 h. Then, LncRNA-HMG was analyzed by RT-qPCR (n = 3). **E** The diagram showing TCF binding elements (TBEs) at the promoter of LncRNA-HMG. **F** ChIP experiment was performed using anti-β-catenin or anti-TCF4 antibodies. The precipitates were subjected to RT-qPCR using the indicated primers. **G** Luciferase reporter assay was performed as indicated. **H** The working model explaining how LncRNA-HMG regulates CRC chemoresistance through inhibiting ferroptosis. All the data are presented as mean ± SD. *P < 0.05, **P < 0.01, ***P < 0.001.

transcription of downstream genes such as *CD44*, *MYC* and *LGR5*, further initiating tumorigenesis [30,43]. We found that LncRNA-HMG is transactivated by Wnt/β-catenin signaling, further indicating the vital roles of LncRNA-HMG in CRC progression. Importantly, LncRNA-HMG acts as a signal between Wnt pathway and p53 pathway. We thus provide LncRNA-HMG as a key regulator in CRC progression. ASO based on LncRNA-HMG shows the ability to alleviate CRC chemoresistance. In the future study, it will be more meaningful to try to develop new drug targeting LncRNA-HMG used in clinical trials.

In summary, we show for the first time that LncRNA-HMG is associated in CRC chemoresistance. Wnt signals upregulate the expression LncRNA-HMG. Subsequently, LncRNA-HMG attenuates p53-mediated ferroptosis, thus facilitating the elimination of ROS or lipid peroxides. Finally, LncRNA-HMG protects CRC cells from ferroptosis. Therefore, LncRNA-HMG might be a potential target for CRC treatment.

4. Materials and methods

4.1. Patients and specimens

The patients diagnosed with CRC and underwent surgical treatment in Peking University Cancer Hospital (PKU Cancer) from 2013 to 2016 were enrolled in this study. Exclusions were made for patients lacking clinical tissue sample, or with incomplete clinicopathological information. The follow-up evaluation for all patients was made until January 1, 2023. Supplementary Table S1 presents the summary of clinical details pertaining to the samples. Written consent was obtained from the participating patients, and the clinical and histopathological data provided to researchers were anonymized. The investigation was approved by the Ethics Committee of Peking University Cancer Hospital & Institute.

4.2. Cell culture and transfection

CRC cell lines including LoVo, HCT116 $p53^{+/+}$, HCT116 $p53^{-/-}$, and SW480 were cultured in DMEM medium supplemented with 10 % fetal bovine serum. The plasmid DNA or siRNA was transfected into cells using Lipofectamine 2000 (Invitrogen, USA) following the manufacturer's instructions. In transient transfection experiments, plasmid DNA remained constant for each group with the empty vector. For the establishment of stable LncRNA-HMG knockdown cell lines, HEK293T cells were transfected with pLKO.1-HMG shRNA or pLKO.1-Ctrl shRNA alongside packaging vectors pMD2.G and psPAX2 to generate lentiviral particles. After harvesting the indicated lentiviruses, LoVo or HCT116 cells were infected with these lentiviruses containing LncRNA-HMG shRNA or control shRNA. Then, puromycin was added for screening the positive stale clones and RT-qPCR was performed for identifying the knockdown efficiency.

4.3. Western blotting and antibodies

Western blotting was conducted following previously established protocols [25]. Primary antibodies targeting anti-SLC7A11/xCT (A2413) and anti-MDM2 (A13327) were purchased from ABclonal Technology (Wuhan, China). Additionally, antibodies including Anti--β-Catenin (9562), Anti-p53 (DO-1), anti-TCF4, and anti-Ub (P4D1) were acquired from Cell Signaling Technology (MA, USA). The antibody anti-VKORC1L1 (abs101967) was purchased from Absin (Shanghai, China).

4.4. Quantitative real-time PCR (RT-qPCR) assay

The total RNAs were isolated from the indicated cells using TRIzol reagent (Invitrogen, USA), followed by purification using the RNeasy Mini Kit (Qiagen, Germany) as per the manufacturer's instructions. cDNA was synthesized from 2 μg of total RNA using the Superscript First-Strand Synthesis System (Yeasen Biotechnology, China). The qPCR was conducted in accordance with the Minimal Information for Publication of Quantitative Real-Time PCR Experiments (MIQE) guidelines. The specific sequences of the qPCR primers were shown in Supplementary Table S5.

4.5. Rapid amplification of cDNA ends (RACE)

RACE was performed using the HiScript-TS 5/3 RACE Kit (Vazyme, China) according to the instruction manual. Briefly, the total RNA was isolated and reverse transcription was conducted using an oligo(dT) primer. The poly(A) tail was then added to the cDNA with Terminal deoxynucleotidyl transferase (TdT). The first round of PCR was performed with an anchor primer and an outer primer. Next, the nested PCR was conducted using a nested gene-specific primer (nested GSP) and an inner primer. The PCR products were analyzed on an agarose gel. Moreover, the products were cloned for sequencing to obtain the complete RNA sequence. The specific sequences of the primers were shown in Supplementary Table S5.

4.6. Immunohistochemistry (IHC) assay

The tissue sections were de-paraffinized in xylene followed by rehydration through a series of graded ethanol. To neutralize the endogenous peroxidase activity, the 0.3 % peroxidase solution was applied to the sections for 30 min. For antigen retrieval, the sections were subjected to boil in citrate buffer at 100 °C for 15 min. Subsequently, after treatment with the blocking buffer, the sections were incubated with the indicated primary antibody overnight at 4 °C. The visualization of the sections was accomplished using the UltraVision Quanto Detection System HRP DAB Kit (ZSGB-Bio, China) following the manufacturer's protocols. Hematoxylin was used for counterstaining, and evaluation was carried out by pathologists who were blinded to the clinical outcome.

4.7. Reduced Glutathione (GSH) assay and Oxidized Glutathione (GSSG) content assay

The relative concentration of GSH and GSSG in cell lysates was determined by utilizing Reduced Glutathione(GSH) Content Assay Kit (Solarbio, China) and Oxidized Glutathione(GSSG) Content Assay Kit (Solarbio, China) following the manufacturer's guidelines. By measuring the absorbance of the resulting at 412 nm using a microplate reader, the GSH and GSSG levels were calculated.

4.8. C11-BODIPY assay

The cells were seeded into 6-well plates, and the culture medium was replaced with serum-free media containing 2 μmol/L C11-BODIPY (Thermo Fisher Scientific, USA) for staining. Subsequently, cells were cultured in the dark for 30 min to assess lipid ROS level. After incubation, cells were detached, washed, and suspended in 400 μl of PBS for flow cytometry analysis using a BD Biosciences instrument. The fluorescence was measured at an excitation wavelength of 488 nm and an emission wavelength of 525 nm. The fluorescence intensity in each group represented the quantity of lipid ROS.

4.9. Malondialdehyde (MDA) assay

The levels of MDA were assessed utilizing Malondialdehyde (MDA) Content Assay Kit (Elabscience, China) in accordance with the provided instructions. About 3×10^6 cells were harvested and the extraction buffer was added to lyse the cells. The lysates were collected. Then, the working solution was added to the lysates and the positive control group. The mixtures were heated at 100 °C for 40 min. After cooling down to room temperature, the reaction mixtures were centrifuged and

the supernatant was transferred to an enzyme-linked immunosorbent assay (ELISA) plate. The OD value was measured at 532 nm. The measured MDA content was then normalized to the protein concentration.

4.10. Reactive oxygen species (ROS) Fluorometric assay

The levels of ROS were assessed by Reactive Oxygen Species (ROS) Fluorometric Assay Kit (Elabscience, China) in accordance with the provided instructions. The culture medium was removed and the cells were washed. The positive control wells (containing TBHP) and negative control wells (without DCFH-DA) were set up. The dye including DCFH-DA was added to the cells and incubated with the cells at 37 °C in the dark for 1 h. Next, the reaction was stopped and the cells were washed three times with wash buffer. The cells were digested and resuspended in wash buffer. Finally, the fluorescence values were measured using fluorescence spectrophotometer.

4.11. Immunoprecipitation assay

The indicated cells were harvested and cell lysates were obtained using Buffer A containing specific components (25 mM Tris-Cl pH 7.5, 150 mM KCl, 1 mM DTT, 2 mM EDTA, 0.5 mM PMSF, and 0.2 % Nonidet P-40). These lysates were directly utilized for immunoprecipitation. Briefly, antibodies were linked with a 50 % suspension of protein A-Sepharose beads (GE Healthcare, USA) in IPP500 solution (500 mM NaCl, 10 mM Tris-Cl pH 8.0, 0.2 % Nonidet P-40). The bead-antibody complexes were then mixed and incubated with the cell lysates for 2 h at 4 °C. After washing, the isolated precipitates were subjected to analysis via Western blot using the specific antibodies.

4.12. Luciferase assay

LoVo and HCT116 cells were plated at a density of 80,000 cells per well. Next, cells were co-transfected with either lncRNA-HMG promoter luciferase reporter or the pGL3-basic reporter control plasmid, alongside a Renilla luciferase control reporter vector (Promega, USA) used to standardize transfection efficiency. Then, luciferase assays were conducted following the manufacturer's guidelines (Dual-Luciferase Reporter Assay System, Promega). The data were presented as relative luciferase activity normalized against the expression of the Renilla luciferase.

4.13. RNA binding protein immunoprecipitation assay (RIP)

The indicated cells were treated with UV light irradiation and subsequently lysed using a high salt lysis buffer (25 mM Tris-Cl pH 7.5, 150 mM KCl, 2 mM EDTA, 0.5 % NP-40, 1 mM NaF, 1 mM DTT, and 100 U/mL RNase inhibitors, along with EDTA-free protease inhibitor). Magnetic beads were coated with 5 mg of anti-p53 or MDM2 antibodies. Then, cell lysates were added and incubated overnight at 4 °C. After reaction, the RNA-protein complexes were washed for six times before digestion with proteinase K. RNA extraction was carried out using Trizol-chloroform RNA extraction methods. The relative RNA expression was assessed via RT-qPCR and normalized against the input. The specific sequences of the primers were shown in Supplementary Table S5.

4.14. RNA pull-down assay

Linearized DNA fragments was prepared through single enzyme digestion of *in vitro* transcription templates. The indicated DNA was purified and used as a template for subsequent *in vitro* transcription. Biotin-labeled RNA (Beyotime, China) is then generated and purified, following overnight incubation. The labeled RNA was prepared and incubated with magnetic beads coated with homogenous streptavidin. After binding and washing, the RNA-protein complexes were eluted and subjected to SDS-PAGE analysis.

4.15. Fluorescence in situ hybridization

The FISH experiment was conducted using the Ribo Fluorescent In Situ Hybridization Kit (RiboBio, China) according to the manufacturer's instructions. Initially, cells were plated on slides and fixed with 4 % paraformaldehyde (PFA) for 15 min at room temperature. Subsequently, the cells underwent permeabilization using 0.5 % Triton X-100. Cy3-labeled probes were then introduced to detect the specific RNAs as indicated, followed by DAPI staining to visualize the nuclei.

4.16. Cell growth assay

Cell growth was assessed following the manufacturer's protocol using Cell Counting Kit (CCK-8) (Yeasen Biotechnology Co., Ltd., China). LoVo and HCT116 cells, transfected with specific shRNAs, were seeded at a density of 1000 cells per well in 96-well plates and cultured in media containing 10 % serum. CCK-8 reagent was introduced to the cells, and the absorbance at 450 nm was measured per day.

4.17. Colony formation assay

The cells were split and counted. Then, 500 cells were seeded into each well of 6-well plates and cultured in media containing 10 % serum for 12 days. Finally, the cells were fixed and stained using crystal violet to count the visible colonies.

4.18. Chromatin immunoprecipitation (ChIP) assay

The Magnetic ChIP Kit from Cell Signaling Technology (Cell Signaling Technology, USA) was used to perform ChIP assay. First, the cells were treated with formaldehyde, facilitating the cross-linking of proteins with genomic DNA. Glycine (0.125 M) was used to halt this process. Then, the cells were collected, centrifuged, and suspended in the lysis buffer (consisting of 1 % SDS, 10 mM EDTA, protease inhibitors, and 50 mM Tris-HCl pH 8.0). The genomic DNA was sonicated to achieve fragments approximately 200–1000 bp in length. The cell lysates were clarified by centrifugation, followed by a 1:10 dilution in ChIP dilution buffer (0.01 % SDS, 1.0 % Triton X-100, 1.2 mM EDTA, 16.7 mM NaCl, protease inhibitors, and 16.7 mM Tris-HCl pH 8.0). Then, the lysates were incubated overnight at 4 °C with rotation along with anti-TCF4 or β-catenin antibodies. ChIP-Grade Protein A/G Magnetic Beads were added to each reaction and incubated for 2 h. Then, the Protein A/G magnetic beads were pelleted by centrifugation and washed sequentially with low salt wash buffer, high salt wash buffer, and LiCl wash buffer. Finally, the beads were washed twice with 1 ml of TE buffer. The reversal of protein-DNA cross-linking was achieved by incubating the beads with 200 mM NaCl and proteinase K for 2 h at 65 °C. DNA was extracted and subjected to RT-qPCR. The input DNA and IgG were utilized for normalization purposes. The specific sequences of the primers were shown in Supplementary Table S5.

4.19. Identification of lncRNA-HMG-binding protein and mass spectrometry analysis

The plasmids containing GFP-tagged-MS2 binding sites and lncRNA-HMG-MS2 were constructed for the experiment. Cells were transfected with the indicated vectors, and cell lysates were prepared in RIPA buffer with protease inhibitors. The lysates were incubated overnight with a GFP antibody, and an IgG antibody was used as a control. Protein complexes were captured using protein A/G magnetic beads, and washed. The precipitates were resolved on SDS-PAGE. The specific protein bands were excised and subjected to mass spectrometry analysis. Mass spectrometry was used to identify proteins differentially associated with lncRNA-HMG, providing insights into potential interacting

partners.

4.20. Animal study

Five-week-old female nude mice were purchased from Beijing Vital River Laboratory Animal Technology Co., Ltd. and the mice were randomly allocated into six groups (n = 6 per group), including LncRNA-HMG-control shRNA, LncRNA-HMG shRNA1, LncRNA-HMG shRNA2, LncRNA-HMG-control shRNA+5-Fu + Oxaliplatin, LncRNA-HMG shRNA1+5-Fu + Oxaliplatin, and LncRNA-HMG shRNA2+5-Fu + Oxaliplatin. The indicated cells were subcutaneously injected into the right flank of each mouse. Then, the mice were treated with an i.p. injection of oxaliplatin (6 mg/kg) and 5-Fu (20 mg/kg) every 3 days. Tumor volume was detected every five days, and calculated using the formula (length × width^2 × 0.5). Thirty-five days later, the mice were sacrificed and xenografts were obtained. The protein level of SLC7A11, VKORC1L1 and p53 was analyzed by Western blot. Animal procedures were approved by the Institutional Animal Care and Use Committee of Peking University Health Science Center (Ethics Approval License, LA2023498).

PDX models were established using fresh tumor samples from CRC patients. Tumor tissues were initially implanted subcutaneously into mice as the first generation (F0). Upon reaching suitable size, tumors were excised, divided, and subcutaneously implanted into mice as the second generation (F2). After the tumor was implanted subcutaneously, tumor-bearing mice were randomly divided into four groups, including LncRNA ASO (10 nmol per injection, RiboBio, China), control ASO, LncRNA ASO combined with oxaliplatin and 5-Fu, and control ASO combined with oxaliplatin and 5-Fu. ASO was administered via intratumoral injection, while 5-Fu (20 mg/kg) and oxaliplatin (6 mg/kg) were administered via intraperitoneal injection. The treatment was conducted every 3 days. Tumor diameter and width in PDX mice were measured every 7 days to calculate tumor volumes ($V = 0.5 \times D \times W^2$; V, volume; D, diameter; W, width). Thirty-five days later, mice were sacrificed. Then, tumor tissues were excised, photographed, weighted, and embedded in paraffin for further pathological analysis.

4.21. Statistical analyses

To assess the significance of differences, we employed one-way ANOVA or a two-tailed Student's t-test. Spearman's correlation coefficient was used to calculate the relationships between the groups. Survival analysis was utilized by Kaplan-Meier analysis, and differences in survival probabilities were determined via the log-rank test. All statistical analyses were conducted using GraphPad Prism or SPSS version 25.0 (SPSS, Inc.). A significance level of $P < 0.05$ was applied for all analyses. Significance levels were denoted as *$P < 0.05$, **$P < 0.01$, ***$P < 0.001$, and ****$P < 0.0001$.

CRediT authorship contribution statement

Zechang Xin: Writing – original draft, Visualization, Data curation, Conceptualization. **Chenyu Hu:** Methodology, Formal analysis. **Chunfeng Zhang:** Validation, Data curation. **Ming Liu:** Resources, Formal analysis. **Juan Li:** Resources, Methodology. **Xiaoyan Sun:** Resources, Formal analysis, Data curation. **Yang Hu:** Visualization, Software, Data curation. **Xiaofeng Liu:** Writing – review & editing, Writing – original draft, Supervision, Investigation, Funding acquisition, Conceptualization. **Kun Wang:** Writing – review & editing, Investigation, Funding acquisition, Conceptualization.

Declaration of competing interest

The authors have declared no conflict of interest.

Data availability

Data will be made available on request.

Acknowledgments

This study was supported by the grants from the Beijing Municipal Natural Science Foundation [Grant No. 7242022], the National Natural Science Foundation of China [Grant No. 82473383], Beijing Capital's Funds for Health Improvement and Research [CFH, 2024-2-2154], and the Beijing Hospitals Authority Youth Programme [Grant No. QML20231109].

Appendix A. Supplementary data

Supplementary data to this article can be found online at https://doi.org/10.1016/j.redox.2024.103362.

References

[1] L.H. Biller, D. Schrag, Diagnosis and treatment of metastatic colorectal cancer: a review, JAMA 325 (7) (2021) 669–685.
[2] D. Xu, X.F. Liu, X.L. Yan, K. Wang, B.C. Xing, Survival prediction in patients with resectable colorectal liver metastases: clinical risk scores and tumor response to chemotherapy, Oncol. Lett. 14 (6) (2017) 8051–8059.
[3] E. Cybulla, A. Vindigni, Leveraging the replication stress response to optimize cancer therapy, Nat. Rev. Cancer 23 (1) (2023) 6–24.
[4] R. Moradi-Marjaneh, S.M. Hassanian, M. Mehramiz, M. Rezayi, G.A. Ferns, M. Khazaei, A. Avan, Reactive oxygen species in colorectal cancer: the therapeutic impact and its potential roles in tumor progression via perturbation of cellular and physiological dysregulated pathways, J. Cell. Physiol. 234 (7) (2019) 10072–10079.
[5] X. Sun, Q. Zhang, X. Lin, P. Shu, X. Gao, K. Shen, Imatinib induces ferroptosis in gastrointestinal stromal tumors by promoting STUB1-mediated GPX4 ubiquitination, Cell Death Dis. 14 (12) (2023) 839.
[6] M. Zhan, Y. Ding, S. Huang, Y. Liu, J. Xiao, H. Yu, L. Lu, X. Wang, Lysyl oxidase-like 3 restrains mitochondrial ferroptosis to promote liver cancer chemoresistance by stabilizing dihydroorotate dehydrogenase, Nat. Commun. 14 (1) (2023) 3123.
[7] G. Lei, Y. Zhang, P. Koppula, X. Liu, J. Zhang, S.H. Lin, J.A. Ajani, Q. Xiao, Z. Liao, H. Wang, B. Gan, The role of ferroptosis in ionizing radiation-induced cell death and tumor suppression, Cell Res. 30 (2) (2020) 146–162.
[8] S. Ouyang, H. Li, L. Lou, Q. Huang, Z. Zhang, J. Mo, M. Li, J. Lu, K. Zhu, Y. Chu, et al., Inhibition of STAT3-ferroptosis negative regulatory axis suppresses tumor growth and alleviates chemoresistance in gastric cancer, Redox Biol. 52 (2022) 102317.
[9] E.C. Cheung, K.H. Vousden, The role of ROS in tumour development and progression, Nat. Rev. Cancer 22 (5) (2022) 280–297.
[10] P. Zhang, C. Zhou, X. Ren, Q. Jing, Y. Gao, C. Yang, Y. Shen, Y. Zhou, W. Hu, F. Jin, et al., Inhibiting the compensatory elevation of xCT collaborates with disulfiram/copper-induced GSH consumption for cascade ferroptosis and cuproptosis, Redox Biol. 69 (2023) 103007.
[11] H. Yang, R.M. Villani, H. Wang, M.J. Simpson, M.S. Roberts, M. Tang, X. Liang, The role of cellular reactive oxygen species in cancer chemotherapy, J. Exp. Clin. Cancer Res. 37 (1) (2018) 266.
[12] Z. Deng, Y. Wang, J. Liu, H. Zhang, L. Zhou, H. Zhao, Y. Han, S. Yan, Z. Dong, Y. Wang, et al., WBP2 restrains the lysosomal degradation of GPX4 to inhibit ferroptosis in cisplatin-induced acute kidney injury, Redox Biol. 65 (2023) 102826.
[13] Z. Wang, N. Shen, Z. Wang, L. Yu, S. Yang, Y. Wang, Y. Liu, G. Han, Q. Zhang, TRIM3 facilitates ferroptosis in non-small cell lung cancer through promoting SLC7A11/xCT K11-linked ubiquitination and degradation, Cell Death Differ. 31 (1) (2024) 53–64.
[14] L. Jiang, N. Kon, T. Li, S.J. Wang, T. Su, H. Hibshoosh, R. Baer, W. Gu, Ferroptosis as a p53-mediated activity during tumour suppression, Nature 520 (7545) (2015) 57–62.
[15] E. Mishima, J. Ito, Z. Wu, T. Nakamura, A. Wahida, S. Doll, W. Tonnus, P. Nepachalovich, E. Eggenhofer, M. Aldrovandi, et al., A non-canonical vitamin K cycle is a potent ferroptosis suppressor, Nature 608 (7924) (2022) 778–783.
[16] X. Yang, Z. Wang, F. Zandkarimi, Y. Liu, S. Duan, Z. Li, N. Kon, Z. Zhang, X. Jiang, B.R. Stockwell, W. Gu, Regulation of VKORC1L1 is critical for p53-mediated tumor suppression through vitamin K metabolism, Cell Metab 35 (8) (2023) 1474–1490 e1478.
[17] M. Chen, C. Zhang, W. Liu, X. Du, X. Liu, B. Xing, Long noncoding RNA LINC01234 promotes hepatocellular carcinoma progression through orchestrating aspartate metabolic reprogramming, Mol. Ther. 30 (6) (2022) 2354–2369.
[18] Y. Zhu, C. Huang, C. Zhang, Y. Zhou, E. Zhao, Y. Zhang, X. Pan, H. Huang, W. Liao, X. Wang, LncRNA MIR200CHG inhibits EMT in gastric cancer by stabilizing miR-200c from target-directed miRNA degradation, Nat. Commun. 14 (1) (2023) 8141.
[19] D. Kumar, S. Gurrapu, Y. Wang, S.Y. Bae, P.R. Pandey, H. Chen, J. Mondal, H. Han, C.J. Wu, S. Karaiskos, et al., LncRNA Malat1 suppresses pyroptosis and T cell-mediated killing of incipient metastatic cells, Nat Cancer 5 (2) (2024) 262–282.

[20] X.M. Yu, S.J. Li, Z.T. Yao, J.J. Xu, C.C. Zheng, Z.C. Liu, P.B. Ding, Z.L. Jiang, X. Wei, L.P. Zhao, et al., N4-acetylcytidine modification of lncRNA CTC-490G23.2 promotes cancer metastasis through interacting with PTBP1 to increase CD44 alternative splicing, Oncogene 42 (14) (2023) 1101–1116.
[21] Y. Zhang, S. Pitchiaya, M. Cieslik, Y.S. Niknafs, J.C. Tien, Y. Hosono, M.K. Iyer, S. Yazdani, S. Subramaniam, S.K. Shukla, et al., Analysis of the androgen receptor-regulated lncRNA landscape identifies a role for ARLNC1 in prostate cancer progression, Nat. Genet. 50 (6) (2018) 814–824.
[22] W. Xue, W. Jian, Y. Meng, T. Wang, L. Cai, Y. Yu, Y. Yu, Z. Xia, C. Zhang, Knockdown of SETD2 promotes erastin-induced ferroptosis in ccRCC, Cell Death Dis. 14 (8) (2023) 539.
[23] H. Wang, Y. Cheng, C. Mao, S. Liu, D. Xiao, J. Huang, Y. Tao, Emerging mechanisms and targeted therapy of ferroptosis in cancer, Mol. Ther. 29 (7) (2021) 2185–2208.
[24] X. Zhang, Q. Zheng, X. Yue, Z. Yuan, J. Ling, Y. Yuan, Y. Liang, A. Sun, Y. Liu, H. Li, et al., ZNF498 promotes hepatocellular carcinogenesis by suppressing p53-mediated apoptosis and ferroptosis via the attenuation of p53 Ser46 phosphorylation, J. Exp. Clin. Cancer Res. 41 (1) (2022) 79.
[25] X. Liu, Y. Tan, C. Zhang, Y. Zhang, L. Zhang, P. Ren, H. Deng, J. Luo, Y. Ke, X. Du, NAT10 regulates p53 activation through acetylating p53 at K120 and ubiquitinating Mdm2, EMBO Rep. 17 (3) (2016) 349–366.
[26] A. Loffreda, E. Jacchetti, S. Antunes, P. Rainone, T. Daniele, T. Morisaki, M. E. Bianchi, C. Tacchetti, D. Mazza, Live-cell p53 single-molecule binding is modulated by C-terminal acetylation and correlates with transcriptional activity, Nat. Commun. 8 (1) (2017) 313.
[27] J. Liu, D. Guan, M. Dong, J. Yang, H. Wei, Q. Liang, L. Song, L. Xu, J. Bai, C. Liu, et al., UFMylation maintains tumour suppressor p53 stability by antagonizing its ubiquitination, Nat. Cell Biol. 22 (9) (2020) 1056–1063.
[28] X. Li, M. Guo, L. Cai, T. Du, Y. Liu, H.F. Ding, H. Wang, J. Zhang, X. Chen, C. Yan, Competitive ubiquitination activates the tumor suppressor p53, Cell Death Differ. 27 (6) (2020) 1807–1818.
[29] H. Yan, W. Wu, Y. Hu, J. Li, J. Xu, X. Chen, Z. Xu, X. Yang, B. Yang, Q. He, P. Luo, Regorafenib inhibits EphA2 phosphorylation and leads to liver damage via the ERK/MDM2/p53 axis, Nat. Commun. 14 (1) (2023) 2756.
[30] X. Liu, K. Su, X. Sun, Y. Jiang, L. Wang, C. Hu, C. Zhang, M. Lu, X. Du, B. Xing, Sec62 promotes stemness and chemoresistance of human colorectal cancer through activating Wnt/beta-catenin pathway, J. Exp. Clin. Cancer Res. 40 (1) (2021) 132.
[31] J.N. Anastas, R.T. Moon, WNT signalling pathways as therapeutic targets in cancer, Nat. Rev. Cancer 13 (1) (2013) 11–26.
[32] C. Hu, Z. Xin, X. Sun, Y. Hu, C. Zhang, R. Yan, Y. Wang, M. Lu, J. Huang, X. Du, et al., Activation of ACLY by SEC63 deploys metabolic reprogramming to facilitate hepatocellular carcinoma metastasis upon endoplasmic reticulum stress, J. Exp. Clin. Cancer Res. 42 (1) (2023) 108.
[33] Y. Tan, J. Li, G. Zhao, K.C. Huang, H. Cardenas, Y. Wang, D. Matei, J.X. Cheng, Metabolic reprogramming from glycolysis to fatty acid uptake and beta-oxidation in platinum-resistant cancer cells, Nat. Commun. 13 (1) (2022) 4554.
[34] A. Tuval, C. Strandgren, A. Heldin, M. Palomar-Siles, K.G. Wiman, Pharmacological reactivation of p53 in the era of precision anticancer medicine, Nat. Rev. Clin. Oncol. 21 (2) (2023) 106–120.
[35] W.Y. Wu, Z.X. Wang, T.S. Li, X.Q. Ding, Z.H. Liu, J. Yang, L. Fang, L.D. Kong, SSBP1 drives high fructose-induced glomerular podocyte ferroptosis via activating DNA-PK/p53 pathway, Redox Biol. 52 (2022) 102303.
[36] Z. Zhang, M. Guo, M. Shen, D. Kong, F. Zhang, J. Shao, S. Tan, S. Wang, A. Chen, P. Cao, S. Zheng, The BRD7-P53-SLC25A28 axis regulates ferroptosis in hepatic stellate cells, Redox Biol. 36 (2020) 101619.
[37] H. Hu, K. Zhao, D. Fang, Z. Wang, N. Yu, B. Yao, K. Liu, F. Wang, Y. Mei, The RNA binding protein RALY suppresses p53 activity and promotes lung tumorigenesis, Cell Rep. 42 (4) (2023) 112288.
[38] A.L. Latif, A. Newcombe, S. Li, K. Gilroy, N.A. Robertson, X. Lei, H.J.S. Stewart, J. Cole, M.T. Terradas, L. Rishi, et al., BRD4-mediated repression of p53 is a target for combination therapy in AML, Nat. Commun. 12 (1) (2021) 241.
[39] Y. Liu, Y. Hou, F. Zhang, X. Wang, ENO1 deletion potentiates ferroptosis and decreases glycolysis in colorectal cancer cells via AKT/STAT3 signaling, Exp. Ther. Med. 27 (4) (2024) 127.
[40] R. Wang, L. Hua, P. Ma, Y. Song, J. Min, Y. Guo, C. Yang, J. Li, H. Su, HSPA5 repressed ferroptosis to promote colorectal cancer development by maintaining GPX4 stability, Neoplasma 69 (5) (2022) 1054–1069.
[41] X. Liu, J. Chen, S. Zhang, X. Liu, X. Long, J. Lan, M. Zhou, L. Zheng, J. Zhou, LINC00839 promotes colorectal cancer progression by recruiting RUVBL1/Tip60 complexes to activate NRF1, EMBO Rep. 23 (9) (2022) e54128.
[42] P. Ding, Y. Xu, L. Li, X. Lv, L. Li, J. Chen, D. Zhou, X. Wang, Q. Wang, W. Zhang, et al., Intracellular complement C5a/C5aR1 stabilizes beta-catenin to promote colorectal tumorigenesis, Cell Rep. 39 (9) (2022) 110851.
[43] C. Zhang, L. Liu, W. Li, M. Li, X. Zhang, C. Zhang, H. Yang, J. Xie, W. Pan, X. Guo, et al., Upregulation of FAM83F by c-Myc promotes cervical cancer growth and aerobic glycolysis via Wnt/beta-catenin signaling activation, Cell Death Dis. 14 (12) (2023) 837.